

Iolanda Lazaro,¹ Ainhoa Oguiza,^{1,2} Carlota Recio,^{1,2} Beñat Mallavia,¹
 Julio Madrigal-Matute,^{1,3} Julia Blanco,⁴ Jesus Egido,^{1,2} Jose-Luis Martin-Ventura,¹
 and Carmen Gomez-Guerrero^{1,2}



Targeting HSP90 Ameliorates Nephropathy and Atherosclerosis Through Suppression of NF- κ B and STAT Signaling Pathways in Diabetic Mice

Diabetes 2015;64:3600–3613 | DOI: 10.2337/db14-1926

Heat shock proteins (HSPs) are induced by cellular stress and function as molecular chaperones that regulate protein folding. Diabetes impairs the function/expression of many HSPs, including HSP70 and HSP90, key regulators of pathological mechanisms involved in diabetes complications. Therefore, we investigated whether pharmacological HSP90 inhibition ameliorates diabetes-associated renal damage and atheroprogession in a mouse model of combined hyperglycemia and hyperlipidemia (streptozotocin-induced diabetic apolipoprotein E-deficient mouse). Treatment of diabetic mice with 17-dimethylaminoethylamino-17-demethoxygeldanamycin (DMAG, 2 and 4 mg/kg, 10 weeks) improved renal function, as evidenced by dose-dependent decreases in albuminuria, renal lesions (mesangial expansion, leukocyte infiltration, and fibrosis), and expression of proinflammatory and profibrotic genes. Furthermore, DMAG significantly reduced atherosclerotic lesions and induced a more stable plaque phenotype, characterized by lower content of lipids, leukocytes, and inflammatory markers, and increased collagen and smooth muscle cell content. Mechanistically, the renoprotective and antiatherosclerotic effects of DMAG are mediated by the induction of protective HSP70 along with inactivation of nuclear factor- κ B (NF- κ B) and signal transducers and activators of transcription (STAT) and target gene expression, both in diabetic mice and in cultured cells under hyperglycemic and proinflammatory conditions. In conclusion, HSP90 inhibition by DMAG restrains the progression of renal and vascular damage in experimental

diabetes, with potential implications for the prevention of diabetes complications.

The prevalence of diabetes has reached epidemic proportions. Nephropathy and atherosclerosis are the major diabetes-driven complications, resulting in disability and increased risk of mortality in diabetic patients. In fact, diabetic nephropathy is the leading cause of end-stage renal disease and also a macrovascular disease risk factor, and atherosclerosis is the main reason for impaired life expectancy in diabetic patients (1,2). Therefore, the prevention of micro- and macrovasculature damage associated with diabetes to improve patient quality of life and life expectancy is a major public health concern. Owing to the fact that current treatment of diabetes is insufficient to avert the complications in a significant proportion of patients, diabetes-associated renal and vascular damage might be counteracted by blocking injury mechanisms and promoting protective and reparative factors. Based on both observational clinical studies and functional evidence from animal models, inflammation is considered a key contributor to the onset and progression of diabetic nephropathy and atherosclerosis, with promising therapeutic opportunities (2,3).

Cellular stress response is directed by the conserved family of heat shock proteins (HSPs) to promote cytoprotection through the transcriptional regulation by heat

¹Renal, Vascular and Diabetes Research Laboratory, IIS-Fundacion Jimenez Diaz, Autonoma University of Madrid, Madrid, Spain

²Spanish Biomedical Research Centre in Diabetes and Associated Metabolic Disorders, Madrid, Spain

³Department of Developmental and Molecular Biology, Institute for Aging Studies, Albert Einstein College of Medicine, Bronx, NY

⁴Department of Pathology, Hospital Clinico San Carlos, Madrid, Spain

Corresponding author: Carmen Gomez-Guerrero, cgomez@fjd.es.

Received 22 December 2014 and accepted 20 June 2015.

This article contains Supplementary Data online at <http://diabetes.diabetesjournals.org/lookup/suppl/doi:10.2337/db14-1926/-/DC1>.

© 2015 by the American Diabetes Association. Readers may use this article as long as the work is properly cited, the use is educational and not for profit, and the work is not altered.

shock transcription factor 1 (HSF1) (4). Given the ubiquity of HSP, it seems unsurprising that these chaperone proteins have been related to many metabolic abnormalities. Evidence from patients and animal models indicate that diabetes differentially modulates the expression of HSP25/27, HSP60, HSP70/72, and HSP90 (5–7), and this may affect the ability of cells to mount an effective cytoprotective response. HSP90, one of the most conserved HSPs, uses the energy generated by ATP binding and hydrolysis to allow folding, maturation, and stability of the so-called “client” proteins involved in cell survival, signal transduction, transcriptional regulation, and innate and adaptive immunity (4). To do so, HSP90 interacts with other cochaperones, forming a multichaperone complex that recognizes client proteins and modulates their activities (4). HSP90 machinery in association with its cochaperone HSP70 is involved in folding and activation of newly synthesized protein kinases, including I κ B kinase (IKK) and Janus kinase (JAK) (8,9). IKK and JAK play, respectively, a key role in the activation of nuclear factor- κ B (NF- κ B) and signal transducers and activators of transcription (STAT), major transcription factors that regulate the expression of many genes involved in inflammation (10,11). This overall prompted the notion of HSP90 as a molecular target of interest for the treatment of several immunological and inflammatory disorders (12,13). So far, most clinical trials of HSP90 inhibitors have focused on cancer therapy (14).

Furthermore, HSP90 inhibitors effectively disrupt HSP90-HSF1 complexes, allowing HSF1 activation and subsequent nuclear translocation to transactivate HSP genes (4,14). Pre-clinical data implicate HSP90 as a promising anti-inflammatory target in rheumatoid arthritis, systemic lupus erythematosus, uveitis, liver injury, and cardiovascular disease models (12,15–18). In diabetic animals, HSP90 inhibition improved insulin sensitivity (19), high-fat diet-induced renal failure (20), and neurodegeneration (21), but the underlying mechanisms involved in these antidiabetic actions are not well defined. Hence, in this work we investigate whether targeting HSP90 delays the progression of diabetes complications in a diabetes mouse model of concomitant renal and macrovascular disease.

RESEARCH DESIGN AND METHODS

Diabetes Model

Animal studies were performed according to the Directive 2010/63/EU of the European Parliament and were approved by the Institutional Animal Care and Use Committee (IIS-Fundacion Jimenez Diaz). Experimental diabetes model of insulin deficiency was induced in 10-week-old male apolipoprotein E-deficient (apoE^{-/-}) mice by two daily intraperitoneal injections of streptozotocin (STZ, 125 mg/kg/day; Sigma-Aldrich, St. Louis, MO) (22–25). Animals maintained on standard diet were monitored every 2–3 days for body weight and nonfasting blood glucose. Severely hyperglycemic mice (blood glucose >29 mmol/L) received insulin (1–1.5 IU) to maintain blood glucose levels within a more tolerable range. Mice with overt diabetes (glucose >19.4 mmol/L)

were randomized to receive 10 weeks of treatment with vehicle (200 μ L saline i.p., every other day; $n = 9$) and 17-dimethylaminoethylamino-17-demethoxygeldanamycin (DMAG; InvivoGen, San Diego, CA) at 2 mg/kg/day ($n = 9$) and 4 mg/kg/day ($n = 6$). Age-matched apoE^{-/-} mice were used as nondiabetic controls (vehicle, $n = 4$; DMAG 4 mg/kg/day, $n = 3$). At the end of the study, 16 h-fasted mice were anesthetized (100 mg/kg ketamine and 15 mg/kg xylazine), saline perfused, and killed. Blood and urine samples were collected for biochemistry.

Histological Analysis

Dissected kidneys were snap-frozen for expression studies or stored in 4% paraformaldehyde for histology. Aortas were divided into two parts: the upper aortic root was embedded in Tissue-Tek O.C.T. Compound (Sakura Finetek Europe, the Netherlands) for histological analysis, and the abdominal/thoracic aorta was processed for mRNA analysis.

Paraffin-embedded kidney sections (3 μ m) were stained with periodic acid Schiff (PAS). Renal lesions were semiquantitatively graded (0–3 scale) in a blinded manner according to the extent of lesions in glomeruli (hypertrophy, hypercellularity, and mesangial expansion; 30 glomeruli per sample), tubules (atrophy and degeneration), and interstitium (fibrosis and infiltration; 20 fields at $\times 40$ per sample). Glomerular area and PAS⁺ mesangial area were quantified by computerized morphometry. Immunodetection of macrophages (F4/80; AbD Serotec, Oxford, U.K.), T cells (CD3; DAKO, Glostrup, Denmark), HSP70 (Abcam), and tyrosine-phosphorylated STAT1 (P-STAT1; Life Technologies, Rockville, MD) and STAT3 (P-STAT3; Santa Cruz Biotechnology, Inc., Santa Cruz, CA) was assessed by immunoperoxidase. Renal fibrosis was determined by picrosirius red staining. Positive staining (>10 fields at $\times 20$ magnification) was quantified using Image Pro-Plus (Media Cybernetics, Bethesda, MD) and expressed as percentage of total area and number of positive cells per glomerular cross-section or interstitial area measured (mm²).

Atherosclerotic lesions in serial 8- μ m aortic sections (covering $\sim 1,000$ μ m from valve leaflets) were quantified by morphometry after Oil Red O/hematoxylin staining. Individual lesion area was determined by averaging the maximal values (approximately three sections). Collagen content was determined by picrosirius red staining. Lesional macrophages (MOMA-2; AbD Serotec, Oxford, U.K.), CD3 T cells, vascular smooth muscle cells (VSMCs) (α -actin-Cy3; Sigma-Aldrich), chemokine (C-C motif) ligand (CCL) 2 (Santa Cruz Biotechnology), CCL5 (Antibodies Online), and tumor necrosis factor α (TNF- α ; Santa Cruz Biotechnology) were detected by immunoperoxidase or immunofluorescence. Positive staining was expressed as percentage of total plaque area or number of positive cells per lesion area (26,27). Activated NF- κ B in kidney and aorta was detected by Southwestern histochemistry using digoxigenin-labeled probes (26,28).

Cell Cultures

Primary mesangial cells (MCs) from mouse kidneys were cultured in RPMI 1640 with 25 mmol/L HEPES, pH 7.4,

supplemented with 10% FBS (22). Murine MC line (SV40 MES 13, CRL-1927; American Type Culture Collection [ATCC], Manassas, VA) was maintained in Dulbecco's modified Eagle's medium (DMEM):F12 medium containing 5% FBS. Murine proximal tubuloepithelial MCT line (29) was cultured in RPMI 1640 containing 10% FBS. Mouse vascular endothelial cell line (MILE SVEN 1, CRL-2279; ATCC) was maintained in DMEM with 5% FBS. Murine bone marrow-derived macrophages were cultured for 7 days in RPMI 1640 with 10% FBS containing 10% L929-cell conditioned medium (23). Murine monocyte/macrophage cell line (RAW 264.7, TIB-71; ATCC) was maintained in DMEM with 10% FBS. All culture media were supplemented with 100 units/mL penicillin, 100 g/mL streptomycin, and 2 mmol/L L-glutamine (Life Technologies). Quiescent cells were pretreated for 4 h with DMAG (5–50 nmol/L) before stimulation with high glucose (HG; 30 mmol/L D-glucose; Sigma-Aldrich) or cytokines (interleukin-6 [IL-6] 10^2 units/mL plus interferon- γ [IFN- γ] 10^3 units/mL; PeproTech, Rocky Hill, NJ). Cell viability was assessed by the 1-(4,5-dimethylthiazol-2-yl)-3,5-diphenylformazan thiazolyl blue formazan (MTT) method.

Transfection of Small Interfering RNA

Cells grown to 60–70% confluence were transfected with 20–30 nmol/L of small interfering RNA (siRNA) targeting HSP70 or negative control scramble siRNA (Ambion) using Lipofectamine RNAiMAX reagent (Life Technologies). Transfected cells (silencing efficiency 50–75%) were pretreated with DMAG for 4 h before 24 h of cytokine stimulation.

mRNA Expression Analysis

Total RNA from mouse tissues (kidney and aorta) and cultured cells was extracted with TRIzol (Life Technologies) and analyzed by real-time quantitative PCR using Taqman gene expression assays (Applied Biosystem, Foster City, CA). Target gene expression was normalized to house-keeping gene (18S).

Protein Expression Analysis

Total cell or kidney whole lysate proteins were resolved on SDS-PAGE gels and immunoblotted for fibronectin (Millipore Corporation, Billerica, MA), HSP32, HSP70 (Enzo Life Sciences, Farmingdale, NY), transforming growth factor- β (TGF- β), HSP27, HSP90, I κ B α (Santa Cruz Biotechnology), P-STAT1 (Life Technologies), and P-STAT3 (Cell Signaling, Beverly, MA), using β -actin (Santa Cruz Biotechnology) or α -tubulin (Sigma-Aldrich) as loading controls. CCL2 and CCL5 protein levels were measured by ELISA (BD Biosciences; R&D Systems, Minneapolis, MN).

Cell Migration Assay

Renal cell chemoattractant capacity was determined using a transwell coculture system (28). In brief, RAW 264.7 cells (1×10^5) were seeded on the upper transwell inserts (8.0- μ m pore size; Merck Millipore, Billerica, MA) and then placed onto a 24-well plate containing MC or MCT cells (5×10^4 per well), which were treated for 4 h with DMAG prior to cytokine stimulation (IL-6 + IFN- γ , 20 h). Cocultures were incubated for a further 8 h, nonmigratory cells were removed from the upper surface of the membrane, and migrated cells were fixed (4% paraformaldehyde), stained (0.2% crystal violet), and counted on 10 randomly selected $\times 200$ fields.

Table 1—Metabolic and renal data in normoglycemic control and diabetic apoE^{-/-} mice after 10 weeks of treatment

	Control		Diabetes		
	Vehicle (n = 4)	DMAG 4 mg/kg (n = 3)	Vehicle (n = 9)	DMAG 2 mg/kg (n = 9)	DMAG 4 mg/kg (n = 6)
Δ BW (g)	2.5 \pm 0.5	2.3 \pm 0.3	-3.3 \pm 0.3	-2.9 \pm 0.1	-1.3 \pm 0.1 $\dagger\dagger$
Blood glucose (mmol/L)	9.2 \pm 0.5	8.7 \pm 0.8	29.3 \pm 0.7 ^{***}	31.1 \pm 1.5 ^{**}	29.6 \pm 2.4 ^{***}
GHbA _{1c} , % (mmol/mol)	ND	ND	3.3 \pm 0.4 (12 \pm 2)	3.3 \pm 0.9 (13 \pm 1)	3.2 \pm 0.6 (11 \pm 4)
Total chol (mmol/L)	8.5 \pm 0.4	9.4 \pm 0.5	15.6 \pm 0.4 ^{***}	17.9 \pm 1.1 ^{***}	14.3 \pm 1.4 [*]
LDL chol (mmol/L)	8.0 \pm 0.4	8.9 \pm 0.5	15.1 \pm 0.4 ^{***}	17.3 \pm 1.1 ^{***}	13.7 \pm 1.4 [*]
HDL chol (mmol/L)	0.33 \pm 0.02	0.30 \pm 0.02	0.29 \pm 0.03	0.20 \pm 0.01 ^{**} , \dagger	0.26 \pm 0.02
TG (mmol/L)	0.62 \pm 0.03	0.62 \pm 0.07	0.86 \pm 0.07	0.86 \pm 0.06	0.62 \pm 0.06
ALT (units/L)	78 \pm 8	68 \pm 9	117 \pm 11	95 \pm 18	80 \pm 19
AST (units/L)	185 \pm 10	110 \pm 16	209 \pm 15	170 \pm 18	176 \pm 34
KBWR (g/kg)	14.8 \pm 0.4	14.7 \pm 0.4	20.5 \pm 1.1 ^{**}	15.0 \pm 0.5 $\dagger\dagger\dagger$	15.3 \pm 0.8 $\dagger\dagger$
SCr (μ mol/L)	11.1 \pm 2.2	8.8 \pm 0.0	36.2 \pm 4.4 ^{***}	19.4 \pm 1.8 $\dagger\dagger$	20.3 \pm 2.6 \dagger
UAC (μ g/ μ mol)	7.2 \pm 0.2	6.9 \pm 0.3	22.6 \pm 1.4 ^{***}	13.0 \pm 0.8 [*] , $\dagger\dagger\dagger$	16.5 \pm 0.8 ^{***} , $\dagger\dagger$
PAS ⁺ mesangial area (%)	4.6 \pm 0.2	4.8 \pm 0.4	14.3 \pm 0.9 ^{***}	9.7 \pm 1.1 [*] , $\dagger\dagger$	8.8 \pm 0.7 $\dagger\dagger$
Glomerular area (μ m ²)	2,188 \pm 107	2,309 \pm 134	4,032 \pm 229	3,080 \pm 214 \dagger	2,379 \pm 213 $\dagger\dagger$

Data are mean \pm SEM. ALT, alanine aminotransferase; AST, aspartate aminotransferase; Δ BW, body weight change (final - initial); chol, cholesterol; KBWR, kidney-to-body weight ratio; ND, not determined; SCr, serum creatinine; TG, triglyceride; UAC, urine albumin-to-creatinine ratio. ^{*}P < 0.05; ^{**}P < 0.01; ^{***}P < 0.001 vs. control-vehicle; \dagger P < 0.05; $\dagger\dagger$ P < 0.01; $\dagger\dagger\dagger$ P < 0.001 vs. diabetes-vehicle.

Statistics

Values are expressed as mean ± SEM. Statistical analyses were performed using Prism 5 (GraphPad Software, Inc., La Jolla, CA). Differences across groups were considered significant at *P* < 0.05 using either nonparametric Mann-Whitney *U* test or one-way ANOVA followed by post hoc Bonferroni pairwise comparison test.

RESULTS

Metabolic and Biochemical Effects of HSP90 Inhibitor in Mice

STZ-induced pancreatic injury in apoE^{-/-} mice represents an insulin-deficient model that combines hyperglycemia and hyperlipidemia. Diabetic apoE^{-/-} mice develop accelerated renal and vascular injury, with similarities to human diabetic nephropathy and atherosclerosis (24,30). We compared the evolution of diabetes in apoE^{-/-} mice after treatment with either vehicle or DMAG at two different concentrations (2 and 4 mg/kg) for 10 weeks. Throughout the study, blood glucose curves were similar in the three diabetic groups (Supplementary Fig. 1). At the end of the study, levels of blood glucose, GHbA_{1c}, total cholesterol, HDL and LDL cholesterol, and triglycerides were all significantly higher in diabetic apoE^{-/-} mice compared with nondiabetic controls, but they were not affected by DMAG treatment (Table 1). Serum transaminase activities were also similar across the groups (Table 1), indicating preserved liver function. As expected, diabetic mice had evidence of enhanced kidney disease, with significant increases in serum creatinine, kidney-to-body weight ratio, and urinary albumin-to-creatinine ratio (Table 1). Interestingly, DMAG

treatment in diabetic animals prevented body weight loss and also significantly decreased serum creatinine, relative kidney weight, and albuminuria (Table 1), reflecting an improved renal function by DMAG.

DMAG Treatment Ameliorates Diabetic Kidney Disease in Mice

Histopathological examination of PAS-stained sections revealed that diabetes caused moderate to severe renal damage in apoE^{-/-} mice, compared with nondiabetic controls (Fig. 1A–C). Furthermore, DMAG treatment dose-dependently ameliorated the renal pathologic changes associated with diabetes, including: 1) glomerular hypertrophy, hypercellularity (mesangial proliferation and infiltrating cells), mesangial matrix expansion, and capillary dilation; 2) tubular atrophy, epithelial dilation, and deposits of glycogen; and 3) interstitial fibrosis and inflammatory infiltrate (Fig. 1A–C and Table 1). DMAG had no significant effect on any parameters measured in nondiabetic controls (Fig. 1A–C and Table 1).

Quantification of F4/80-positive macrophages (Fig. 2A) and CD3-positive T cells (Fig. 2B) demonstrated a marked decrease (~60%) in the number of infiltrating cells in both glomeruli and interstitium of diabetic mice treated with DMAG, compared with the vehicle-treated group. Consistently, DMAG reduced the gene expression levels of monocyte and T-cell chemokines (CCL2 and CCL5) and proinflammatory cytokine TNF-α in diabetic kidneys, with significant effect at the highest dose (% decrease vs. vehicle: 59 ± 8, 45 ± 12, and 85 ± 3, respectively; *P* < 0.05)

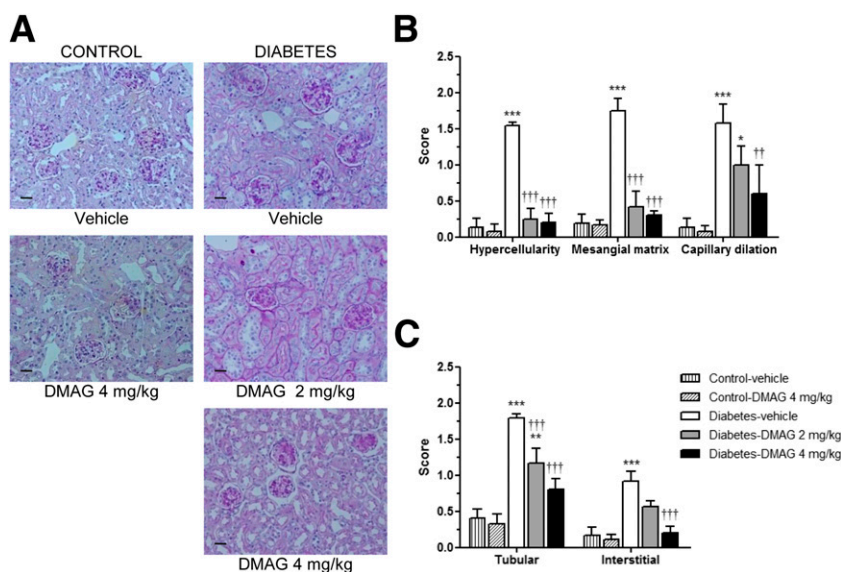


Figure 1—DMAG protects from diabetes-associated renal injury in apoE^{-/-} mice. A: Representative images (scale bar, 20 μm) of PAS-stained kidney sections from nondiabetic control and diabetic apoE^{-/-} mice treated with vehicle or DMAG (2 and 4 mg/kg) for 10 weeks. Semiquantitative assessments of lesions in glomeruli (B) and tubulointerstitial compartment (C). Vertical striped bars indicate control-vehicle mice (*n* = 4); hatched bars, control-DMAG 4 mg/kg (*n* = 3); white bars, diabetes-vehicle (*n* = 9); gray bars, diabetes-DMAG 2 mg/kg (*n* = 9); black bars, diabetes-DMAG 4 mg/kg (*n* = 6). Data are mean ± SEM. **P* < 0.05, ***P* < 0.01, and ****P* < 0.001 vs. control-vehicle group; ††*P* < 0.01 and †††*P* < 0.001 vs. diabetes-vehicle group.

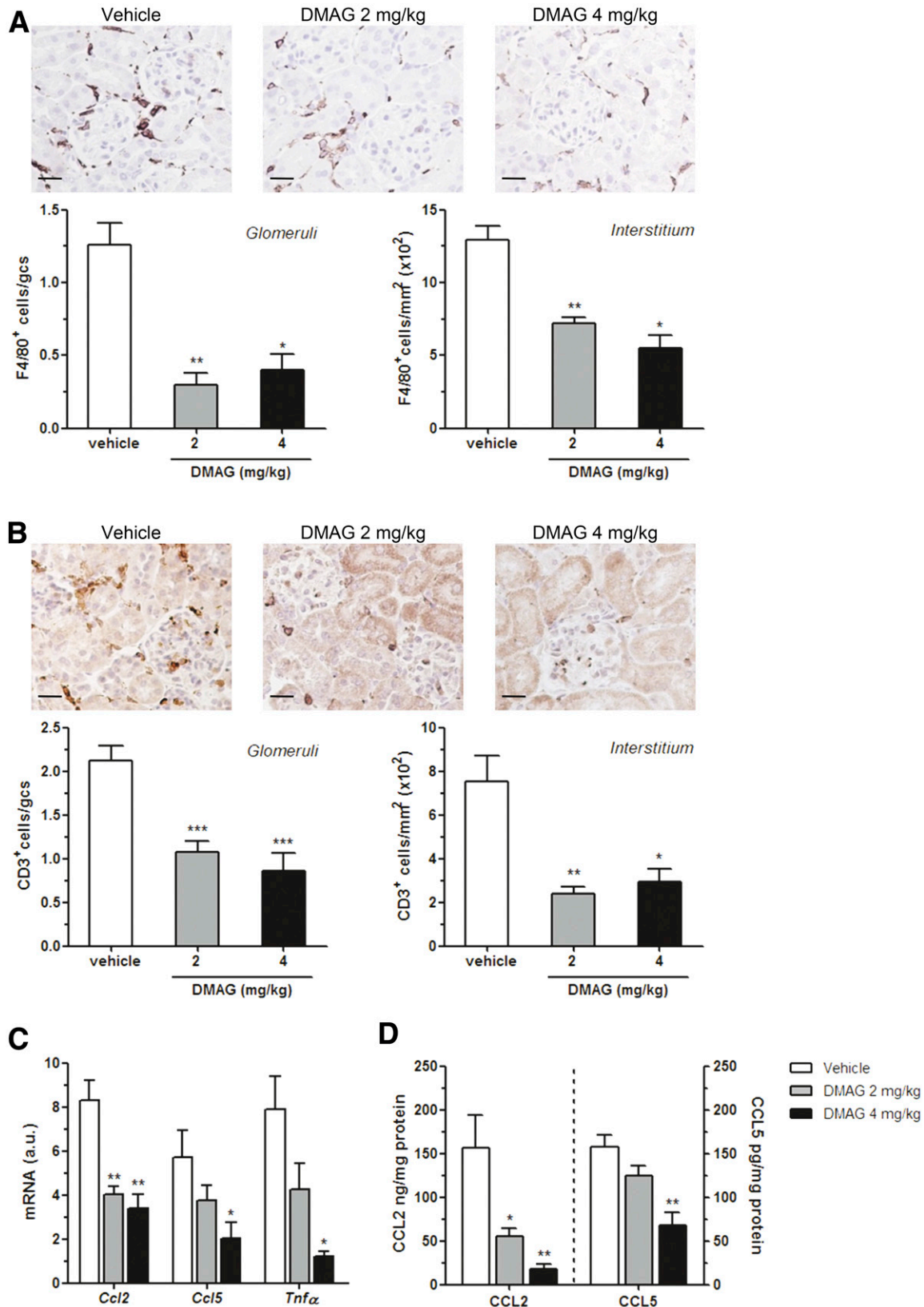


Figure 2—Attenuated inflammation in kidneys from DMAG-treated diabetic mice. Immunoperoxidase images (scale bar, 20 μm) of F4/80⁺ macrophages (A) and CD3⁺ T-cell (B) staining in kidney samples from diabetic apoE^{-/-} mice. Bottom panels: Quantification of mononuclear cell infiltration in glomeruli and interstitium. C: Real-time PCR analysis of inflammatory gene expression in renal cortex from diabetic mice. Values normalized by 18S are expressed in arbitrary units (a.u.). D: CCL2 and CCL5 protein expression in the renal cortical lysates from diabetic mice were measured by ELISA. The dashed line is a separation between CCL2 and CCL5 data. White bars indicate diabetes-vehicle

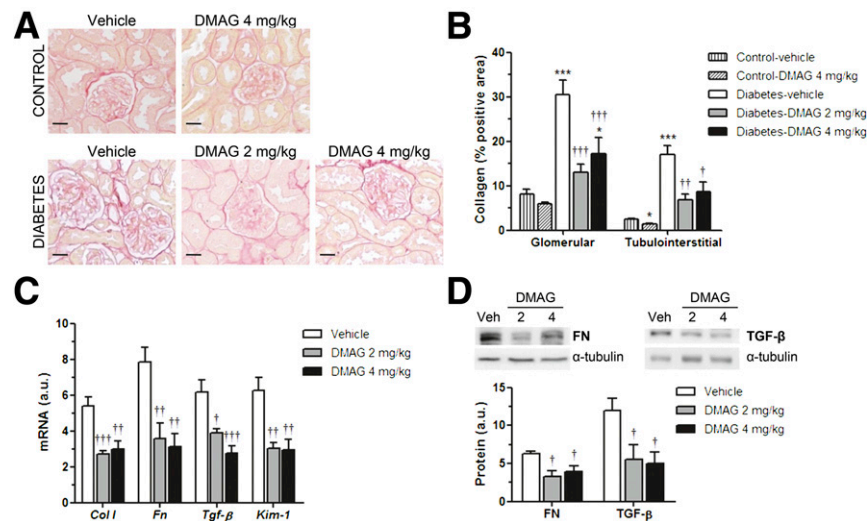


Figure 3—DMAG reduces renal fibrosis in diabetic apoE^{-/-} mice. **A**: Representative images (scale bar, 20 μ m) of picosirius red staining in renal sections from nondiabetic control and diabetic apoE^{-/-} mice treated with vehicle or DMAG (2 and 4 mg/kg) for 10 weeks. **B**: Quantitative analysis of collagen-positive area in glomerular and tubulointerstitial compartments. **C**: Real-time PCR analysis of mRNA expression of type I collagen (*Col 1*), fibronectin (*Fn*), profibrotic factor (*Tgf- β*), and tubular injury marker (*Kim-1*) in renal cortex from diabetic mice. Values normalized by 18S are expressed in arbitrary units (a.u.). **D**: Western blot analyses of fibronectin (FN) and TGF- β expression in renal cortical lysates from diabetic mice. Shown are representative blots and the summary of normalized densitometric quantification. Vertical striped bars indicate control-vehicle mice ($n = 4$); hatched bars, control-DMAG 4 mg/kg ($n = 3$); white bars, diabetes-vehicle ($n = 9$); gray bars, diabetes-DMAG 2 mg/kg ($n = 9$); black bars, diabetes-DMAG 4 mg/kg ($n = 6$). Data are mean \pm SEM. * $P < 0.05$ and *** $P < 0.001$ vs. control-vehicle group; † $P < 0.05$, †† $P < 0.01$, and ††† $P < 0.001$ vs. diabetes-vehicle group. Veh, vehicle.

(Fig. 2C). Chemokine protein levels in diabetic kidneys were also found significantly decreased in DMAG groups (Fig. 2D).

To assess the extent of renal fibrosis, we measured the collagen content by picosirius red staining in kidney sections from nondiabetic and diabetic mice. DMAG effectively reduced the glomerular and tubulointerstitial fibrosis in diabetic apoE^{-/-} mice without significant effect in nondiabetic controls (Fig. 3A and B). Furthermore, diabetic mice treated with DMAG exhibited significantly lower levels of extracellular matrix proteins (type I collagen and fibronectin) and profibrotic factor TGF- β than the vehicle-treated group (Fig. 3C and D). DMAG also suppressed the renal expression of kidney injury molecule-1 (Kim-1) (Fig. 3C), a sensitive biomarker of tubular injury in several kidney diseases.

HSP90 Inhibition Modulates HSP70 Expression and Inflammatory Signaling Pathways in Diabetic Kidneys

To assess the efficiency of DMAG on HSP90 inhibition, we studied the effects on its cochaperone HSP70, which is upregulated as a result of the blockage of the ATP-binding site of HSP90 (14). As expected, DMAG upregulated the mRNA and protein expression of HSP70 (~2–3.5-fold increase vs. vehicle), but not HSP90, in diabetic kidneys, with a wide distribution in both glomerular and tubular

regions of DMAG-treated mice (Supplementary Fig. 2A–C).

Among the different HSP90-associated proteins, we further analyzed whether DMAG modulates renal activation of NF- κ B and STAT, key intracellular pathways in the regulation of inflammatory and fibrotic genes (3). In situ Southwestern histochemistry revealed an intense nuclear localization of activated NF- κ B in glomerular and tubulointerstitial cells of diabetic mice, and a dose-dependent inhibition by DMAG treatment (Fig. 4A–C). DMAG administration also prevented STAT1 and STAT3 activation in diabetic kidneys, as demonstrated by immunodetection of tyrosine-phosphorylated proteins (Fig. 4A–D).

Impact of DMAG on Diabetes-Associated Atherosclerosis

Quantification of aortic root sections after Oil Red O/hematoxylin staining (Fig. 5A–C) revealed that the induction of diabetes exacerbates atherosclerosis in apoE^{-/-} mice (2.5-fold increase in area compared with nondiabetic controls) and also demonstrates the atheroprotective effect of DMAG. In fact, DMAG attenuated atherosclerosis in nondiabetic apoE^{-/-} mice (Fig. 5A and B), as previously reported (17). Remarkably, atherosclerotic plaques of diabetic mice with DMAG treatment exhibited a dose-dependent

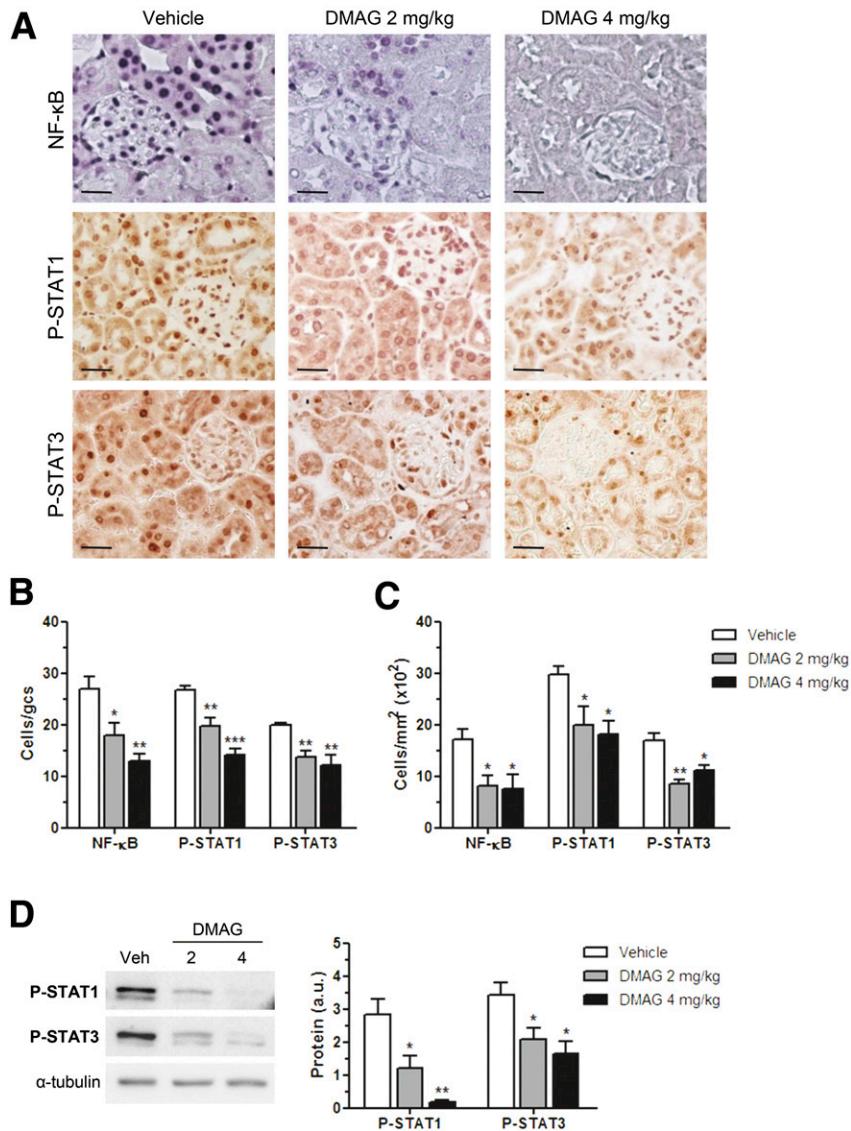


Figure 4—HSP90 inhibition attenuates NF-κB and STAT in diabetic kidneys. In situ detection of activated NF-κB (Southwestern histochemistry) and phosphorylated STAT proteins (P-STAT1 and P-STAT3; immunoperoxidase) in kidney sections from diabetic apoE^{-/-} mice after 10 weeks of treatment with vehicle or DMAG (2 and 4 mg/kg). Representative micrographs (A) (scale bar, 20 μm) and quantification of positive staining in glomerular (B) and tubulointerstitial (C) compartments are shown. D: Western blot analyses of P-STAT1 and P-STAT3 in renal cortical lysates from diabetic mice. Shown are representative images and the summary of normalized quantification, expressed in arbitrary units (a.u.). White bars indicate diabetes-vehicle mice; gray bars, diabetes-DMAG 2 mg/kg; black bars, diabetes-DMAG 4 mg/kg. Data are mean ± SEM (*n* = 6–9 animals per group). **P* < 0.05, ***P* < 0.01, and ****P* < 0.001 vs. diabetes-vehicle group. gcs, glomerular cross-section; Veh, vehicle.

decrease in the lesion size (Fig. 5B), extension (Fig. 5C), and neutral lipid content (% Oil Red O-positive area: vehicle, 23.9 ± 3.9 ; DMAG 2 mg/kg, 15.1 ± 1.2 ; DMAG 4 mg/kg, 4.2 ± 1.2 ; *P* < 0.05 vs. vehicle; not shown).

Accumulation of monocytes/macrophages (MOMA-2) (Fig. 5D) and T cells (CD3) (Fig. 5E) within the atherosclerotic plaques of diabetic mice was reduced by DMAG treatment, with significant effect at high dose (% inhibition vs. vehicle: 58 ± 9 and 56 ± 13 , respectively; *P* < 0.02). Furthermore, analysis of collagen (picosirius red staining) and VSMC (α-actin immunofluorescence) content in atherosclerotic plaques from DMAG-treated diabetic mice

showed a more stable phenotype, with significant raises in the relative proportions of collagen to lipids and VSMCs to macrophages when compared with vehicle-treated diabetic mice (Fig. 5F).

The anti-inflammatory effect of DMAG in diabetic atherosclerosis was also evidenced by a marked decrease in the activation of NF-κB (Fig. 6A) and the expression of CCL2 (Fig. 6B), CCL5 (Fig. 6C), and TNF-α (Fig. 6D) in plaques of DMAG-treated compared with vehicle-treated mice. In addition, quantitative real-time PCR analysis on RNA from aorta presented notable reductions in gene expression of CCL2, CCL5,

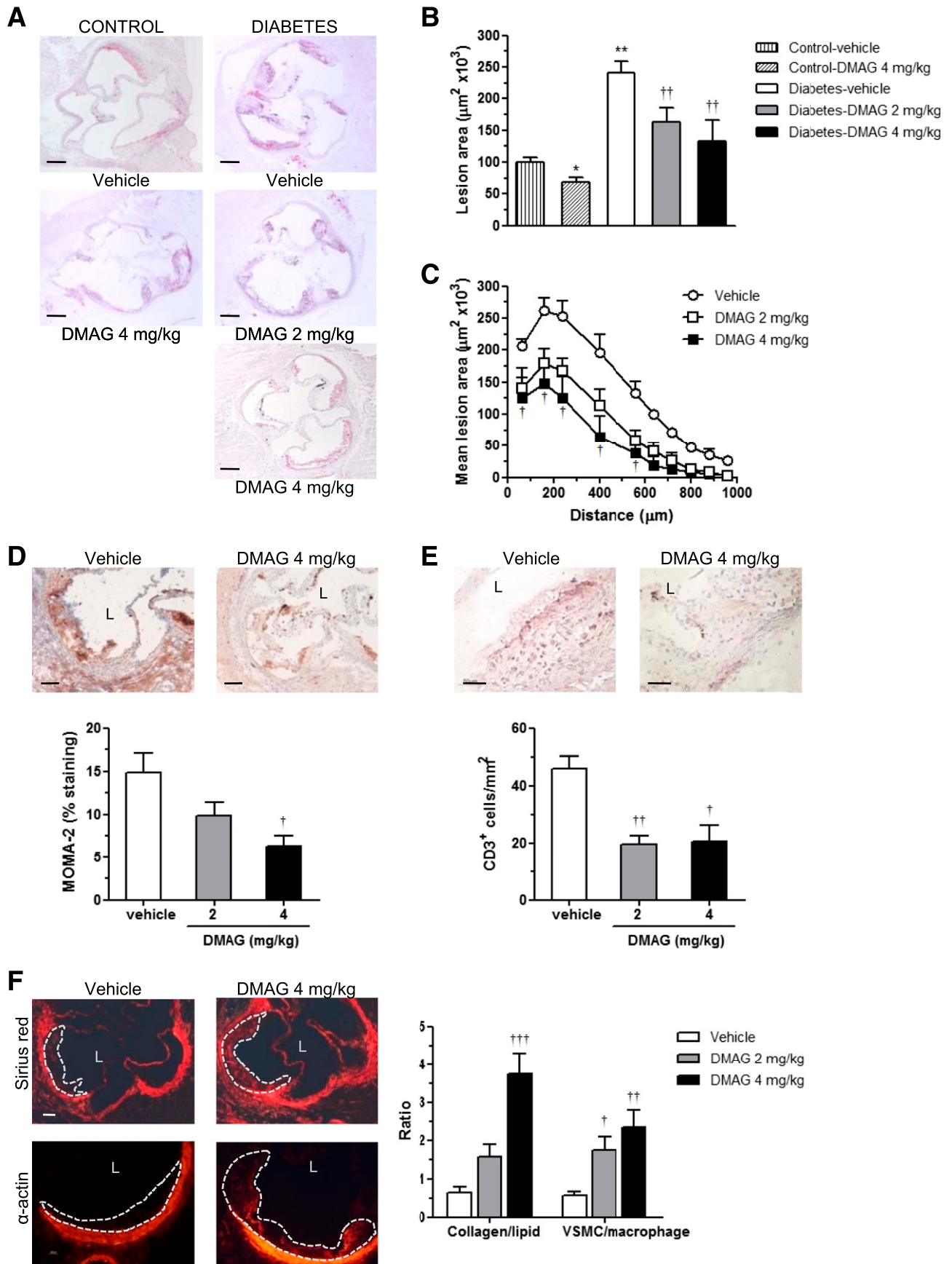


Figure 5—DMAG therapy alters the size and composition of atherosclerotic plaques in diabetic mice. **A**: Representative images of Oil Red O/hematoxylin-stained aortic root sections from nondiabetic control and diabetic apoE^{-/-} mice after 10 weeks of treatment with vehicle or

and TNF- α as a result of DMAG treatment (Fig. 6E). Furthermore, DMAG treatment resulted in a dose-dependent induction of HSP70 mRNA expression in mouse aorta (Fig. 6E).

In Vitro Analysis of DMAG in Renal and Vascular Cells

The in vitro effects of DMAG on NF- κ B and STAT activation and target gene expression were investigated in renal cells, vascular endothelial cells, and macrophages stimulated under hyperglycemic (HG) or proinflammatory (IL-6 + IFN- γ) conditions, in an attempt to mimic the diabetic milieu.

In the tubuloepithelial MCT cell line and primary macrophages, DMAG prevented HG-induced NF- κ B activation, as evidenced by increased protein levels of inhibitory I κ B α subunit (Fig. 7A). Similarly, DMAG pretreatment inhibited the degradation of I κ B α in cytokine-stimulated MCT (Supplementary Fig. 3A), whereas no effect was observed with DMAG alone. Confocal microscopy experiments further revealed that DMAG reduced the nuclear translocation of the p65 subunit in vascular endothelial cells exposed to HG (Fig. 7B). We also observed that DMAG prevented the phosphorylation of STAT1 and STAT3 proteins in both HG-stimulated macrophages (Fig. 7C) and cytokine-stimulated renal cells (Fig. 7D and Supplementary Fig. 3B). Cell viability remained unaffected under these experimental conditions (Supplementary Fig. 3C).

We next examined the role of HSP90 inhibition on the expression of NF- κ B/STAT-dependent genes (e.g., CCL2 and type I collagen) induced by hyperglycemia or inflammation. In cytokine-stimulated renal cells, DMAG pretreatment resulted in a significantly reduced mRNA expression of CCL2 and type I collagen (Fig. 7E). DMAG also prevented CCL2 protein secretion (Supplementary Fig. 3E) and led to a lower macrophage chemoattractant capacity of renal cells, as determined by a migration assay in a coculture system (% inhibition vs. cytokines: 56 ± 2 and 78 ± 4 , respectively; $P < 0.02$) (Fig. 7F). Similarly, DMAG was also able to prevent HG-induced CCL2 expression in MCT, macrophages, and endothelial cells (Supplementary Fig. 3D).

The involvement of HSP70 in DMAG-mediated cellular effects was further explored by genetic silencing in renal cells. First, we observed that DMAG dose-dependently increased both gene (Supplementary Fig. 4A) and protein (Supplementary Fig. 4B) expression of HSP family members, predominantly HSP70, and to a lesser degree HSP32 and HSP27. In addition, cell transfection with HSP70 siRNA markedly

reduced HSP70 expression, without affecting HSP90 levels (Supplementary Fig. 5). We also observed that HSP70 silencing increased the cellular susceptibility to inflammatory stimulation, as demonstrated by a 2.5-fold higher *Ccl2* mRNA expression in HSP70-silenced cells compared with cells transfected with a control scrambled siRNA (Fig. 7G). Remarkably, DMAG was not able to significantly inhibit the cytokine-dependent *Ccl2* mRNA expression in HSP70-silenced cells (Fig. 7G), providing evidence that the beneficial effect associated with HSP90 inhibition is partially due to the induction of HSP70 expression.

DISCUSSION

Alterations in cellular homeostasis, signaling pathways, and gene expression operate concurrently to develop diabetic vascular derangements, such as nephropathy and atherosclerosis. Diabetes is associated with defects in HSP function mediated by either transcriptional or posttranslational mechanisms that regulate cellular levels of HSP in a tissue-specific manner, and such impairments contribute to diabetes complications, thus resulting in a vicious cycle (31,32). The role of HSP90 extends beyond heat shock response owing to its chaperoning function to fold and stabilize many client proteins involved in cell proliferation, differentiation, apoptosis, and inflammation, and is therefore proposed as an important target in immunity and inflammation (4). In this report, we demonstrate that pharmacological HSP90 inhibition ameliorates diabetes-associated renal damage and atheroprogession through the attenuation of cellular processes regulated by NF- κ B and STAT signaling pathways, therefore indicating that HSP90 is a therapeutic target in diabetes complications.

HSP90 inhibitors such as geldanamycin and its derivatives targeting HSP90 N terminus and blocking its ATPase activity have emerged as a clinically relevant strategy in cancer and are also promising drugs for immune and inflammatory diseases, including diabetes (14). Our results in a well-established mouse model of combined hyperglycemia and hyperlipidemia (STZ-induced diabetic apoE^{-/-} mice) demonstrate that HSP90 inhibition by DMAG effectively improved renal function, as evidenced by reduced serum creatinine and urine albumin-to-creatinine ratio, without overt side effects and toxicity. Unlike a previous study that shows reversed hyperglycemia by HSP90 inhibitors in diet-induced obese mice (19), we observed that DMAG administration did not

DMAG (2 and 4 mg/kg). *B*: Average of maximal lesion area in each group. *C*: Extent of atherosclerotic lesions throughout the studied region in diabetic mice (vehicle, white circles; DMAG 2 mg/kg, white squares; DMAG 4 mg/kg, black squares). *D* and *E*: Representative micrographs and quantification of macrophages (MOMA-2) (*D*) and T cells (CD3) (*E*) in the atherosclerotic plaques of diabetic mice. *F*: Assessment of plaque stability by the detection of collagen (picosirius red staining) and VSMC (α -actin immunofluorescence) in diabetic mouse aortas. Representative images and quantification of collagen-to-lipid ratio (picosirius red area/Oil Red O area) and VSMC-to-macrophage ratio (α -actin area/MOMA-2 area) are shown. Vertical striped bars indicate control-vehicle mice ($n = 4$); hatched bars, control-DMAG 4 mg/kg ($n = 3$); white bars, diabetes-vehicle ($n = 9$); gray bars, diabetes-DMAG 2 mg/kg ($n = 9$); black bars, diabetes-DMAG 4 mg/kg ($n = 6$). Data are mean \pm SEM. * $P < 0.05$ and ** $P < 0.01$ vs. control-vehicle group; † $P < 0.05$, †† $P < 0.01$, and ††† $P < 0.001$ vs. diabetes-vehicle group. Scale bars: 200 μ m (*A*) and 50 μ m (*D-F*). Dashed lines, atheroma plaques. L, lumen.

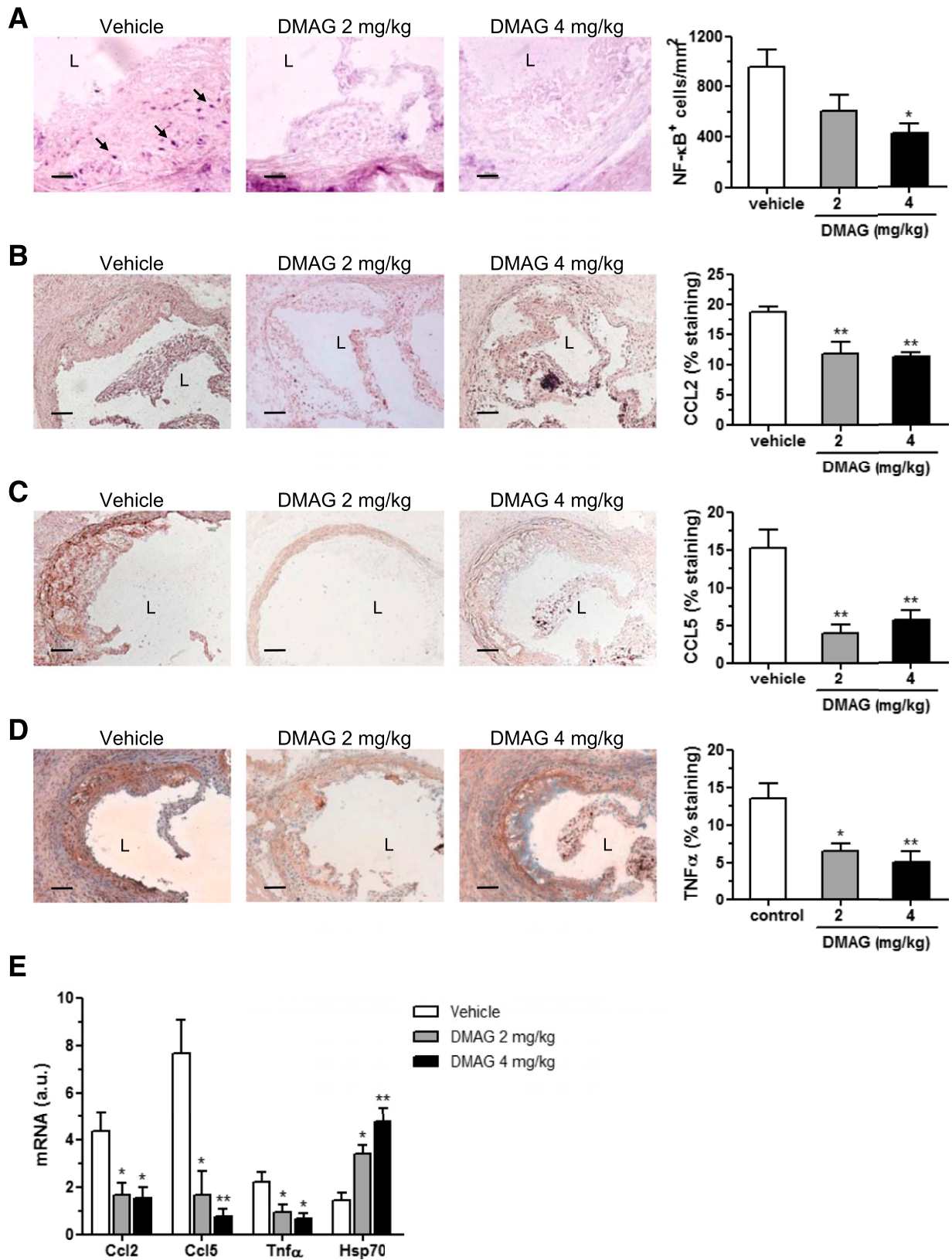


Figure 6—Reduced inflammation in atherosclerotic plaques of DMAG-treated mice. *A*: In situ detection of activated NF-κB by Southwestern histochemistry in aortic sections of diabetic apoE^{-/-} mice. Representative images (scale bar, 20 μm; arrows, positive staining) and quantification of positive cells per lesion area. *B–D*: Immunoperoxidase images (scale bar, 50 μm; L, lumen) of CCL2 (*B*), CCL5 (*C*), and TNF-α (*D*) staining in diabetic mouse aortas and quantification of positive staining per lesion area. *E*: Real-time PCR analysis of the indicated genes in aortic tissue. Values normalized by 18S are expressed in arbitrary units (a.u.). White bars indicate diabetes-vehicle mice; gray bars, diabetes-DMAG 2 mg/kg; black bars, diabetes-DMAG 4 mg/kg. Data are the mean ± SEM (six to nine animals per group). **P* < 0.05 and ***P* < 0.01 vs. diabetes-vehicle group.

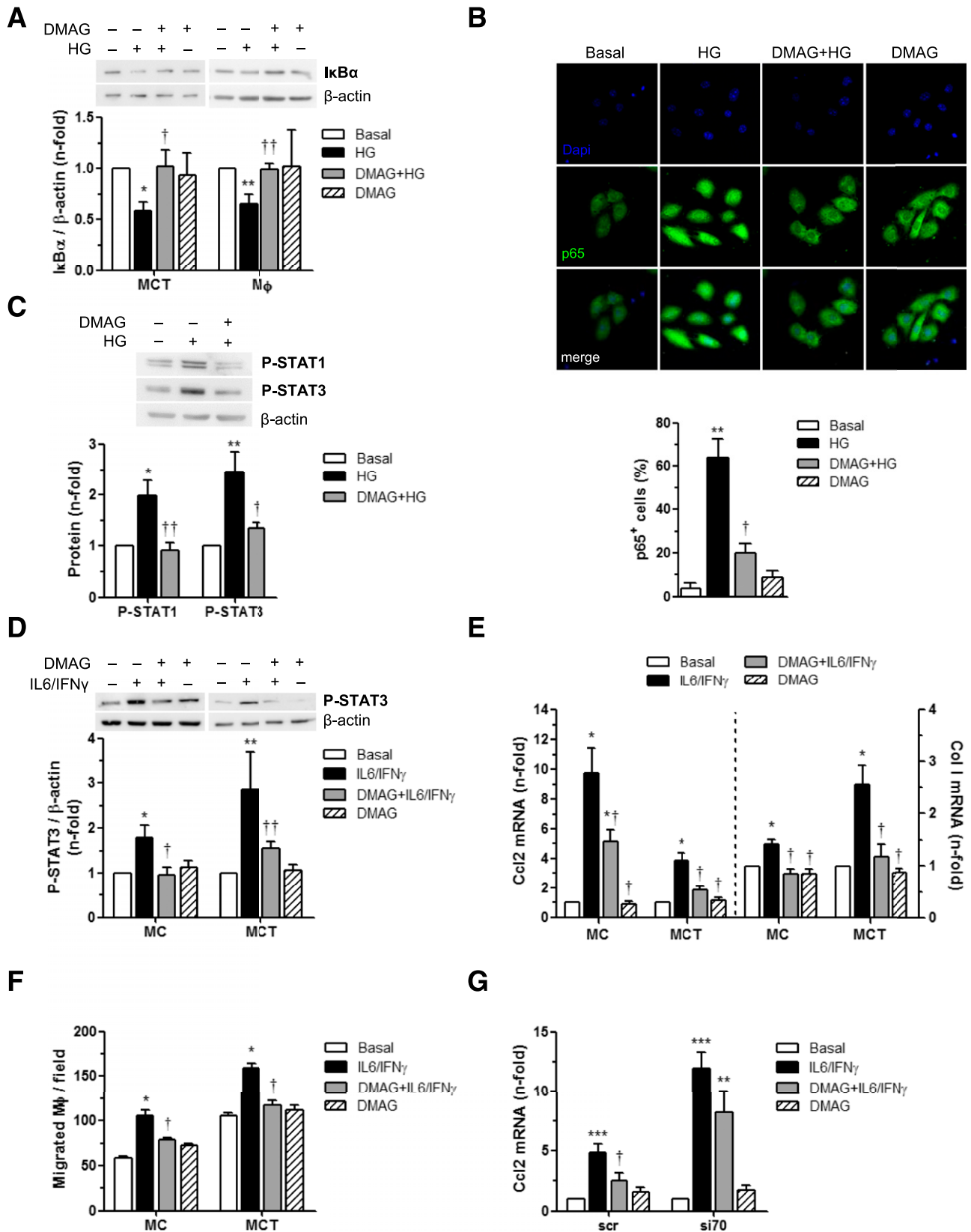


Figure 7— In vitro effects of DMAG treatment in renal and vascular cells. Quiescent cells were pretreated with DMAG (50 nmol/L, 4 h) prior to stimulation with either cytokines (IL-6 10² units/mL and IFN- γ 10³ units/mL) or HG (β -glucose 30 mmol/L) at different time points. **A:** Western blot analysis in total cell extracts from MCT and macrophages (M ϕ), showing that DMAG prevents I κ B α degradation induced by 6 h of HG stimulation. **B:** Representative confocal images of p65 NF- κ B subunit localization in endothelial cells and quantification of p65-positive nuclei after 2 h of HG stimulation. Western blot analyses of P-STAT1/P-STAT3 in total cell extracts from HG-stimulated macrophages (6 h) (**C**) and cytokine-stimulated MC and MCT (1 h) (**D**). **E:** Real-time PCR analysis of *Ccl2* and type I collagen (*Col 1*) gene

affect the metabolic severity of diabetes, with no changes in hyperglycemia, lipid profile, and body weight. Of note, DMAG treatment attenuated the structural pathologic changes in the diabetic kidney, including glomerular hyperplasia and mesangial matrix expansion, as well as tubular atrophy, interstitial fibrosis, and inflammation, hallmarks of end-stage renal failure. In line with the recently reported effect of HSP90 inhibitor on high-fat diet-induced renal failure in diabetes (20), our work adds differences in treatment dose and duration and study samples and provides mechanistic details about the renoprotective action of DMAG in diabetic mice.

Diabetes-associated inflammation promotes a progressive accumulation of kidney leukocytes (33) that contribute to the development and progression of diabetic nephropathy either by direct interaction with the renal cells or by releasing cytokines and growth factors involved in cell proliferation, migration, and extracellular matrix production (34,35). Besides renal histological improvement, we also found a marked anti-inflammatory and antifibrotic effect of HSP90 inhibition. In fact, DMAG-treated mice exhibited reduced macrophage and T-cell infiltration along with a decreased expression of proinflammatory genes (TNF- α , CCL2, and CCL5). Previous reports indicated that HSP90 inhibitors prevent inflammatory gene expression in different cell types, including cancer cells (36), leukocytes (17,37), and renal and vascular cells (15,17). In line with this, our studies in cultured mesangial and tubular cells mimicking hyperglycemic and inflammatory diabetic conditions demonstrated that DMAG inhibited the gene expression and protein secretion of CCL2 and also mitigated macrophage chemotaxis, further substantiating the *in vivo* findings. Moreover, we observed that DMAG protected from the development of renal fibrosis in diabetic mice, with significant reductions in the expression of extracellular matrix proteins and profibrotic factor TGF- β . These observations were further confirmed *in vitro* by analyzing the expression of an extracellular matrix protein (type I collagen) in renal cells. In agreement with the previously reported ability of DMAG to inhibit TGF- β signaling *in vitro* (38) and to reduce renal fibrosis in mice (39), our findings point toward HSP90 as an attractive target to attenuate renal inflammation and fibrosis in diabetic nephropathy.

Our data highlight a potential use of HSP90 inhibitors for prevention of diabetes-associated atherosclerosis. Indeed, DMAG administration dose-dependently reduced the size and extension of atherosclerotic lesions in STZ-induced diabetic apoE^{-/-} mice and also altered plaque composition without any incidence in lipid profile. Increased HSP90 expression

has been linked to vulnerability of human advanced atherosclerotic lesions, and therefore it has been suggested as a promising target to stabilize atheroma plaques through the modulation of inflammation and oxidative stress (17,18,40). Our observations in diabetic mice revealed that DMAG treatment promoted a less inflamed, more stable phenotype characterized by lower content of lipids, macrophages, and T cells and higher collagen and VSMC content. Additionally, atherosclerotic lesions of DMAG-treated mice displayed a lower amount of NF- κ B-activated cells together with a downregulation in the aortic expression of cytokines and chemokines involved in proatherogenic activation of vessel cells. Our *in vitro* studies performed in macrophages and endothelial cells, two of the cell types involved in atherosclerosis progression, demonstrated that DMAG impaired inflammatory gene expression in a hyperglycemic environment. These results are in agreement with the recently reported antimigratory effect of HSP90 inhibitor during atherogenesis (41).

Our study provides *in vivo* and *in vitro* evidence that DMAG inhibits NF- κ B and STAT, two representative HSP90-regulated pathways that control key pathological mechanisms involved in diabetes complications. Owing to its chaperoning function, HSP90 regulates the stability and the activation of NF- κ B and STAT signaling pathways by direct association and stabilization of their respective activating kinases, IKK (42) and JAK2 (43). Accordingly, the efficacy of HSP90 inhibitors in animal models has been linked to the disruption of the IKK complex and JAK2 protein stability, further inhibiting downstream transcription factors such as p50/p65 NF- κ B (44) and STAT1/STAT3/STAT5 (45). Dysregulated NF- κ B and STAT pathways contribute to diabetic nephropathy and atherosclerosis by inducing the transcription of many genes associated with inflammation, renal fibrosis (45–47), and the proatherogenic state (23,48). We have previously tested a number of potential novel approaches (e.g., kinase inhibitors, permeable peptides, and gene therapy) to tackle diabetic nephropathy and atherosclerosis by separately inhibiting the STAT and NF- κ B pathways (23,26,28,29). Here, we demonstrated that DMAG treatment resulted in combined inhibition of the NF- κ B and STAT pathways and subsequent downregulation of their inducible genes (e.g., cytokines, chemokines, and extracellular matrix proteins) both in diabetic mice and *in vitro*. Given that HSP90 inhibitors degrade many different client proteins, it is likely that the protective effects of DMAG on diabetic mice may result from inhibition of multiple target proteins in renal and vascular cells.

Another established effect of HSP90 inhibition is the induction of HS70 expression through the activation of

expression in MC and MCT stimulated with cytokines at 8 h. Values were normalized to 18S. *F*: Transwell cell migration assay of RAW 264.7 macrophages to cytokine-stimulated renal MC and MCT. *G*: Real-time PCR analysis of *Cc12* gene expression in MCT cells transfected (20–30 nmol/L, 24 h) with either scrambled (scr) or specific siRNA for HSP70 (si70) and stimulated overnight with cytokines. *A*, *C*, and *D*: Representative immunoblots and summary of normalized densitometric quantification are shown. *E* and *G*: Real-time PCR data were normalized to 18S. Values represent the mean \pm SEM of three to six independent experiments. White bars indicate basal condition; black bars, stimulus (cytokine or HG); gray bars, DMAG+stimulus; and hatched bars, DMAG alone. **P* < 0.05, ***P* < 0.01, and ****P* < 0.001 vs. basal; †*P* < 0.05 and ††*P* < 0.01 vs. stimulus.

HSF1, resulting from HSP90-HSF1 complex disruption (14,19). HSP70 is likely to confer protection against disturbed metabolic homeostasis via multiple modes of action, including reduced inflammation (49) and improved insulin sensitivity (19). In agreement with previous descriptions (38,50), we demonstrate that DMAG treatment dose-dependently induced HSP70 expression in kidneys and aorta of diabetic mice and in cultured cells. Interestingly, we also observed that HSP70 gene silencing enhanced cytokine responsiveness of cells and partially attenuated the inhibitory effect of DMAG, thus suggesting that DMAG-mediated HSP70 induction contributes to cytoprotection and counterbalance of diabetes-induced cell damage.

Collectively, our experimental data provide the first evidence that HSP90 inhibition simultaneously ameliorates diabetes-associated nephropathy and atherosclerosis through the induction of protective HSP70 and the attenuation of the NF- κ B and STAT pathways, thus resulting in improved renal inflammation and fibrosis and stabilization of atherosclerotic plaques. Therefore, we propose HSP90 inhibition as a novel intervention to limit diabetes-associated complications.

Acknowledgments. The authors thank Dr. M.D. Sanchez-Niño (Nephrology Department, IIS-Fundacion Jimenez Diaz) for helpful advice on the siRNA experiments.

Funding. This work was supported by grants from the Spanish Ministry of Economy and Competitiveness (SAF2012-38830 and SAF2010-21852), the Spanish Ministry of Health (FS PI14/00386 and DiabetesCancerConnect PIE13/00051), the Spanish Societies of Nephrology and Atherosclerosis, and the Iñigo Alvarez de Toledo Renal Foundation. I.L. was supported by a postdoctoral fellowship from FIS (Sara Borrell program).

Duality of Interest. No potential conflicts of interest relevant to this article were reported.

Author Contributions. I.L. designed experiments, researched and analyzed data, and wrote the manuscript. A.O. and C.R. researched and analyzed data and critically revised the manuscript. B.M., J.M.-M., and J.B. researched, analyzed, or interpreted data. J.E. and J.-L.M.-V. critically revised the manuscript for important intellectual content. C.G.-G. conceived and designed the study, analyzed data, and drafted and reviewed the manuscript. C.G.-G. is the guarantor of this work and, as such, had full access to all the data in the study and takes responsibility for the integrity of the data and the accuracy of the data analysis.

References

- Nathan DM. Long-term complications of diabetes mellitus. *N Engl J Med* 1993;328:1676–1685
- Rask-Madsen C, King GL. Vascular complications of diabetes: mechanisms of injury and protective factors. *Cell Metab* 2013;17:20–33
- Fernandez-Fernandez B, Ortiz A, Gomez-Guerrero C, Egido J. Therapeutic approaches to diabetic nephropathy—beyond the RAS. *Nat Rev Nephrol* 2014;10:325–346
- Taipale M, Jarosz DF, Lindquist S. HSP90 at the hub of protein homeostasis: emerging mechanistic insights. *Nat Rev Mol Cell Biol* 2010;11:515–528
- Kurucz I, Morva A, Vaag A, et al. Decreased expression of heat shock protein 72 in skeletal muscle of patients with type 2 diabetes correlates with insulin resistance. *Diabetes* 2002;51:1102–1109
- Tessari P, Puricelli L, Iori E, et al. Altered chaperone and protein turnover regulators expression in cultured skin fibroblasts from type 1 diabetes mellitus with nephropathy. *J Proteome Res* 2007;6:976–986
- Barutta F, Pinach S, Giunti S, et al. Heat shock protein expression in diabetic nephropathy. *Am J Physiol Renal Physiol* 2008;295:F1817–F1824
- Caplan AJ, Mandal AK, Theodoraki MA. Molecular chaperones and protein kinase quality control. *Trends Cell Biol* 2007;17:87–92
- Li J, Buchner J. Structure, function and regulation of the hsp90 machinery. *Biomed J* 2013;36:106–117
- Lawrence T. The nuclear factor NF- κ B pathway in inflammation. *Cold Spring Harb Perspect Biol* 2009;1:a001651
- Adhikari N, Charles N, Lehmann U, Hall JL. Transcription factor and kinase-mediated signaling in atherosclerosis and vascular injury. *Curr Atheroscler Rep* 2006;8:252–260
- Rice JW, Veal JM, Fadden RP, et al. Small molecule inhibitors of Hsp90 potentially affect inflammatory disease pathways and exhibit activity in models of rheumatoid arthritis. *Arthritis Rheum* 2008;58:3765–3775
- Kakeda M, Arock M, Schlapbach C, Yawalkar N. Increased expression of heat shock protein 90 in keratinocytes and mast cells in patients with psoriasis. *J Am Acad Dermatol* 2014;70:683–690.e1
- Hong DS, Banerji U, Tavana B, George GC, Aaron J, Kurzrock R. Targeting the molecular chaperone heat shock protein 90 (HSP90): lessons learned and future directions. *Cancer Treat Rev* 2013;39:375–387
- Shimp SK 3rd, Chafin CB, Regna NL, et al. Heat shock protein 90 inhibition by 17-DMAG lessens disease in the MRL/lpr mouse model of systemic lupus erythematosus. *Cell Mol Immunol* 2012;9:255–266
- Ambade A, Catalano D, Lim A, Mandrekar P. Inhibition of heat shock protein (molecular weight 90 kDa) attenuates proinflammatory cytokines and prevents lipopolysaccharide-induced liver injury in mice. *Hepatology* 2012;55:1585–1595
- Madrigal-Matute J, López-Franco O, Blanco-Colio LM, et al. Heat shock protein 90 inhibitors attenuate inflammatory responses in atherosclerosis. *Cardiovasc Res* 2010;86:330–337
- Madrigal-Matute J, Fernandez-Garcia CE, Gomez-Guerrero C, et al. HSP90 inhibition by 17-DMAG attenuates oxidative stress in experimental atherosclerosis. *Cardiovasc Res* 2012;95:116–123
- Lee JH, Gao J, Kosinski PA, et al. Heat shock protein 90 (HSP90) inhibitors activate the heat shock factor 1 (HSF1) stress response pathway and improve glucose regulation in diabetic mice. *Biochem Biophys Res Commun* 2013;430:1109–1113
- Zhang HM, Dang H, Kamat A, Yeh CK, Zhang BX. Geldanamycin derivative ameliorates high fat diet-induced renal failure in diabetes. *PLoS One* 2012;7:e32746
- Urban MJ, Pan P, Farmer KL, Zhao H, Blagg BS, Dobrowsky RT. Modulating molecular chaperones improves sensory fiber recovery and mitochondrial function in diabetic peripheral neuropathy. *Exp Neurol* 2012;235:388–396
- Lopez-Parra V, Mallavia B, Lopez-Franco O, et al. Fc γ receptor deficiency attenuates diabetic nephropathy. *J Am Soc Nephrol* 2012;23:1518–1527
- Recio C, Oguiza A, Lázaro I, Mallavia B, Egido J, Gomez-Guerrero C. Suppressor of cytokine signaling 1-derived peptide inhibits Janus kinase/signal transducers and activators of transcription pathway and improves inflammation and atherosclerosis in diabetic mice. *Arterioscler Thromb Vasc Biol* 2014;34:1953–1960
- Chew P, Yuen DY, Stefanovic N, et al. Antiatherosclerotic and renoprotective effects of ebselen in the diabetic apolipoprotein E/GP1-double knockout mouse. *Diabetes* 2010;59:3198–3207
- Engler FA, Zheng B, Balthasar JP. Investigation of the influence of nephropathy on monoclonal antibody disposition: a pharmacokinetic study in a mouse model of diabetic nephropathy. *Pharm Res* 2014;31:1185–1193
- López-Franco O, Hernández-Vargas P, Ortiz-Muñoz G, et al. Parthenolide modulates the NF- κ B-mediated inflammatory responses in experimental atherosclerosis. *Arterioscler Thromb Vasc Biol* 2006;26:1864–1870
- Ortiz-Muñoz G, Martín-Ventura JL, Hernandez-Vargas P, et al. Suppressors of cytokine signaling modulate JAK/STAT-mediated cell responses during atherosclerosis. *Arterioscler Thromb Vasc Biol* 2009;29:525–531
- Mallavia B, Recio C, Oguiza A, et al. Peptide inhibitor of NF- κ B translocation ameliorates experimental atherosclerosis. *Am J Pathol* 2013;182:1910–1921

29. Ortiz-Muñoz G, Lopez-Parra V, Lopez-Franco O, et al. Suppressors of cytokine signaling abrogate diabetic nephropathy. *J Am Soc Nephrol* 2010;21:763–772
30. Hsueh W, Abel ED, Breslow JL, et al. Recipes for creating animal models of diabetic cardiovascular disease. *Circ Res* 2007;100:1415–1427
31. Yamagishi N, Nakayama K, Wakatsuki T, Hatayama T. Characteristic changes of stress protein expression in streptozotocin-induced diabetic rats. *Life Sci* 2001;69:2603–2609
32. Atalay M, Oksala N, Lappalainen J, Laaksonen DE, Sen CK, Roy S. Heat shock proteins in diabetes and wound healing. *Curr Protein Pept Sci* 2009;10:85–95
33. Galkina E, Ley K. Leukocyte recruitment and vascular injury in diabetic nephropathy. *J Am Soc Nephrol* 2006;17:368–377
34. Chow FY, Nikolic-Paterson DJ, Ozols E, Atkins RC, Rollin BJ, Tesch GH. Monocyte chemoattractant protein-1 promotes the development of diabetic renal injury in streptozotocin-treated mice. *Kidney Int* 2006;69:73–80
35. Navarro-González JF, Mora-Fernández C. The role of inflammatory cytokines in diabetic nephropathy. *J Am Soc Nephrol* 2008;19:433–442
36. Kolosenko I, Grander D, Tamm KP. IL-6 activated JAK/STAT3 pathway and sensitivity to Hsp90 inhibitors in multiple myeloma. *Curr Med Chem* 2014;21:3042–3047
37. Bae J, Munshi A, Li C, et al. Heat shock protein 90 is critical for regulation of phenotype and functional activity of human T lymphocytes and NK cells. *J Immunol* 2013;190:1360–1371
38. Yun CH, Yoon SY, Nguyen TT, et al. Geldanamycin inhibits TGF- β signaling through induction of Hsp70. *Arch Biochem Biophys* 2010;495:8–13
39. Noh H, Kim HJ, Yu MR, et al. Heat shock protein 90 inhibitor attenuates renal fibrosis through degradation of transforming growth factor- β type II receptor. *Lab Invest* 2012;92:1583–1596
40. Businaro R, Profumo E, Tagliani A, et al. Heat-shock protein 90: a novel autoantigen in human carotid atherosclerosis. *Atherosclerosis* 2009;207:74–83
41. Kim J, Jang SW, Park E, Oh M, Park S, Ko J. The role of heat shock protein 90 in migration and proliferation of vascular smooth muscle cells in the development of atherosclerosis. *J Mol Cell Cardiol* 2014;72:157–167
42. Salminen A, Paimela T, Suuronen T, Kaarniranta K. Innate immunity meets with cellular stress at the IKK complex: regulation of the IKK complex by HSP70 and HSP90. *Immunol Lett* 2008;117:9–15
43. Marubayashi S, Koppikar P, Taldone T, et al. HSP90 is a therapeutic target in JAK2-dependent myeloproliferative neoplasms in mice and humans. *J Clin Invest* 2010;120:3578–3593
44. Hertlein E, Wagner AJ, Jones J, et al. 17-DMAG targets the nuclear factor-kappaB family of proteins to induce apoptosis in chronic lymphocytic leukemia: clinical implications of HSP90 inhibition. *Blood* 2010;116:45–53
45. Marrero MB, Banes-Berceli AK, Stern DM, Eaton DC. Role of the JAK/STAT signaling pathway in diabetic nephropathy. *Am J Physiol Renal Physiol* 2006;290:F762–F768
46. Mezzano S, Aros C, Droguett A, et al. NF-kappaB activation and overexpression of regulated genes in human diabetic nephropathy. *Nephrol Dial Transplant* 2004;19:2505–2512
47. Brosius FC 3rd. New insights into the mechanisms of fibrosis and sclerosis in diabetic nephropathy. *Rev Endocr Metab Disord* 2008;9:245–254
48. Baker RG, Hayden MS, Ghosh S. NF- κ B, inflammation, and metabolic disease. *Cell Metab* 2011;13:11–22
49. Chung J, Nguyen AK, Henstridge DC, et al. HSP72 protects against obesity-induced insulin resistance. *Proc Natl Acad Sci U S A* 2008;105:1739–1744
50. Harrison EM, Sharpe E, Bellamy CO, et al. Heat shock protein 90-binding agents protect renal cells from oxidative stress and reduce kidney ischemia-reperfusion injury. *Am J Physiol Renal Physiol* 2008;295:F397–F405